



Research Article

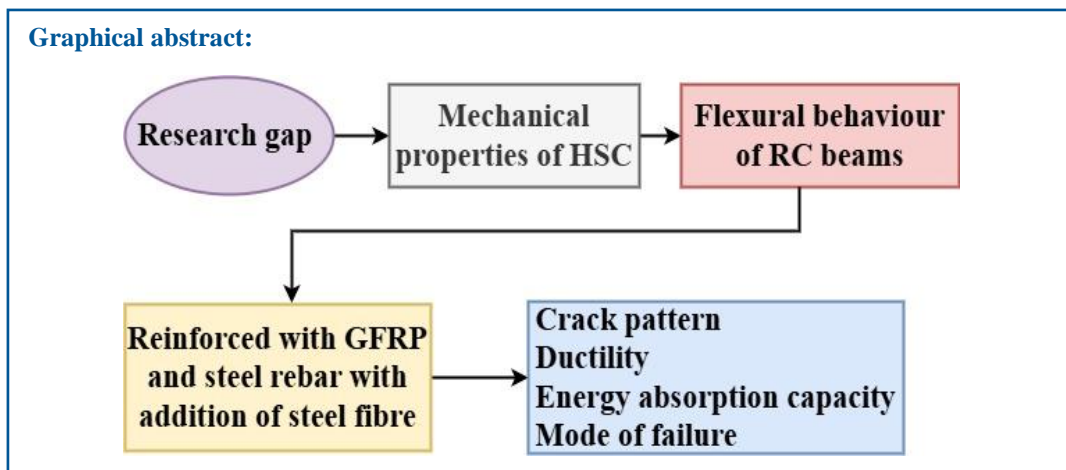
A comparative study between the flexural behaviour of high-strength steel fiber concrete beams reinforced with glass fibre reinforced polymer (GFRP) and steel bars

Sasikumar P. ¹*

¹ K.Ramakrishnan College of Technology, Anna University, Tamil Nadu (India); sasikumar.p.civil@krct.ac.in
*Correspondence: sasikumar.p.civil@krct.ac.in

Received: 25.04.24; **Accepted:** 11.02.26; **Published:** 10.03.26

Citation: Sasikumar, P. (2026). A comparative study between the flexural behaviour of high-strength steel fibre concrete beams reinforced with glass fibre reinforced polymer (GFRP) and steel bars. *Revista de la Construcción. Journal of Construction*, 25(1), 30-49. <https://doi.org/10.7764/RDLC.25.1.30>



Highlights:

- The flexural behaviour of the RC beams was examined with the addition of steel fibres.
- The steel fibres improved the energy absorption capacity of the RC beams.
- Additionally, GFRP rebar has improved ductility behaviour compared to steel rebar.
- GFRP rebar is an alternative material for steel rebar.
- This research proposes practical applications in the construction industry.

Abstract: Glass fibre reinforced polymer (GFRP) rebar is an alternative material to traditional rebar. GFRP rebar exhibits superior ductility and corrosion resistance compared to steel reinforcement. This study investigated the flexural behaviour of eight GFRP- and steel-reinforced concrete beams with dimensions of 150mm x 200mm x 2500mm, subjected to two-point loading. The flexural behaviour of RC beams reinforced with High-Strength Concrete (HSC) was investigated. The control and optimum average cube compressive strengths are 81.64 MPa and 83.42 MPa, respectively. Both steel and GFRP RC beams were examined, with the addition of 0.6% steel fibre. The main objectives of this study encompassed the

specimens' load-carrying capacity, failure mode, ductility, stiffness, and energy absorption capacity. Notably, GFRP RC beams demonstrated superior load-carrying capacity and ductility compared to steel RC beams. Additionally, the mid-span deflection of the RC beams was evaluated using two codes: ACI 440.1R and CSA S806. Furthermore, proposed a method to predict mid-span deflection, and our experimental results closely aligned with the predictions.

Keywords: High-strength concrete, steel fibre, proposed method, ductility, energy absorption capacity.

Abbreviation:

ACI: American concrete institute

ASTM: American society for testing and materials

B: Breadth

CA: Coarse aggregate

CC: Concrete crushing

CS: Compressive strength

CSA: Canadian standards association

D: Depth

E: Energy absorption

FA: Fine aggregate

FRP: Fibre reinforced polymer

GFRP: Glass fibre reinforced polymer

HSC: High strength concrete

IS: Indian standard

L: Length

RC: Reinforced concrete

SF: Shear failure

SF: Steel fibre

SF: Steel fibre

SP: Superplasticizer

T: Tone

W/B: Water binding ratio

1. Introduction

The construction industry has been using GFRP rebar extensively as a substitute for conventional steel rebar due to the latter's ongoing deterioration. The GFRP rebar offers excellent corrosion resistance, a favourable weight ratio, high strength, and ductility compared to steel rebars (Ge et al., 2020; Zeng et al., 2020; Cao et al., 2020; Zeng et al., 2021a; Guo et al., 2018; Guo et al., 2020; Guo et al., 2020a). However, GFRP rebars have a lower modulus of elasticity than steel rebars, resulting in a linear stress-strain curve and brittleness (Chaallal and Benmokrane, 1996; Abdalla, 2002). FRP bars are commonly used in RC sleepers (Ferdous et al., 2021; Manalo et al., 2010; Salih et al., 2021), columns, and beams (Raza et al., 2021; Nakano et al., 1993; Toutanji et al., 2000; Sasikumar and Manju, 2022; Sasikumar and Manju, 2023; Sasikumar and Manju, 2024). Extensive research has been conducted on RC beams reinforced with FRP rebar (Alsayed et al., 2000; Ahmed et al., 2020; Saleh et al., 2019; Goldston et al., 2017; Hadi et al., 2017; Hasan et al., 2018; El-Nemr et al., 2018; Junaid et al., 2019; Liu et al., 2019; Yo et al., 2021; Abdallah et al., 2020), enhancing the durability of structures (Nanni et al., 2014; Schutte, 1994; Wang, and Belarbi, 2011).

Nevertheless, RC beams reinforced with FRP bars typically exhibit lower serviceability performance than those reinforced with steel bars due to FRP bars' lower modulus of elasticity and inferior ductility (Adam et al., 2015). The experimental results for GFRP-reinforced RC beams demonstrated superior flexural and ductility behaviour compared to steel-reinforced RC beams (Lau et al., 2010). To compare the performance of concrete beams reinforced with hybrid bars to beams that were only steel reinforced, to study the flexural behaviour of the former. The hybrid beams exhibited ultimate load capacities comparable to those of steel-reinforced beams. GFRP bars significantly contributed to the load-carrying capacity, dispelling concerns about their strength. Although hybrid beams displayed slightly lower initial stiffness due to the lower modulus of elasticity of GFRP bars, cracking patterns were similar in both beams, with flexural cracks forming near mid-span. GFRP bars exhibited limited ductility but maintained serviceability. In contrast, steel-reinforced beams showed higher ductility during post-cracking stages (Qu et al., 2009).

Aydin et al. (2019) studied hybrid beams combining GFRP box profiles, concrete, and steel bars. These innovative beams exhibited significantly enhanced flexural performance compared to classical reinforced concrete beams. The flexural strength of the improved hybrid beams increased approximately twofold, and fracture toughness improved by 53%. Similarly, (Gu et al., 2021) explored the tensile properties of steel-FRP composite bars (SFCBs) and their bonding behaviour with concrete in chloride-corrosive environments. Their findings contribute valuable insights for practical applications in construction. The flexural behaviour of various concrete beams, including ordinary steel bars, steel-fibre-reinforced polymer composite bars (SFRP), pure fibre-reinforced polymer bars, and hybrid bars. SFRP bar beams demonstrated stable post-yield stiffness, while ordinary reinforced concrete beams had lower ultimate loads than SFRP bar beams. Hybrid beams (reinforced with steel and basalt fibre-reinforced polymer bars) carried an ultimate load of approximately 72% compared to SFRP bars due to premature slip of basalt fibre-reinforced polymer. The energy ductility coefficient is a reasonable measure for evaluating the performance of SFRP bar beams. Adjusting the steel-fibre-reinforced polymer ratio and fibre-reinforced polymer type can achieve high initial stiffness and good ductility in SFRP bar-reinforced concrete beams. SFRP bar-reinforced concrete beams exhibit high durability due to the outer fibre-reinforced polymer layer (Sun et al., 2012).

Concrete columns reinforced with a combination of hybrid steel and GFRP bars exhibited greater resistance to cyclic lateral loads than those reinforced solely with steel or GFRP (Tavakol & Kazemi, 2025). The advanced predictive models for shear stress and angular strain in panels reinforced with GFRP emphasizing improved analytical precision (Carrillo et al., 2025). The importance of durability and structural integrity, noting that hybrid reinforcement combinations improve long-term performance (Prakash et al., 2025). The beams reinforced with both steel and GFRP bars retain their strength under both static and cyclic loads. Together, these studies highlight the promise of hybrid reinforcement strategies in achieving a balance of strength, ductility, and durability in concrete structures. They also indicate a growing consensus that integrating GFRP reduces corrosion risks while maintaining structural resilience (Sidhardhan & Madaswamy (2025).

The literature reviewed highlights the innovative nature of hybrid reinforcement techniques in concrete structures, where GFRP rebars are increasingly utilized as corrosion-resistant substitutes for steel. However, they face limitations due to their

lower modulus of elasticity and ductility. Researchers have advanced this area by combining GFRP with steel or other FRPs, achieving a balance of strength, ductility, and durability while addressing serviceability concerns. Cutting-edge designs, such as GFRP box profiles and steel-FRP composite bars, have demonstrated significant improvements in flexural strength, fracture toughness, and bonding performance under corrosive conditions. Additionally, investigations into hybrid beams and columns reveal their exceptional performance under both static and cyclic loads, with predictive models further enhancing the analytical accuracy regarding shear and strain behaviour. Together, these advancements clearly illustrate the novelty of hybrid reinforcement, which not only reduces corrosion risks but also improves long-term durability, providing a sustainable solution for resilient concrete infrastructure. The current literature indicates considerable advances in the application of GFRP and hybrid reinforcement systems; however, significant research gaps remain. The majority of studies focus on flexural behaviour and durability, with insufficient attention to long-term serviceability, fatigue performance, and large-scale structural applications under realistic loading and environmental conditions. Additionally, there is a need to enhance predictive models to accurately capture the intricate interactions among steel, GFRP, and other FRP types, which opens opportunities for thorough experimental validation and analytical frameworks that connect laboratory results with real-world applications.

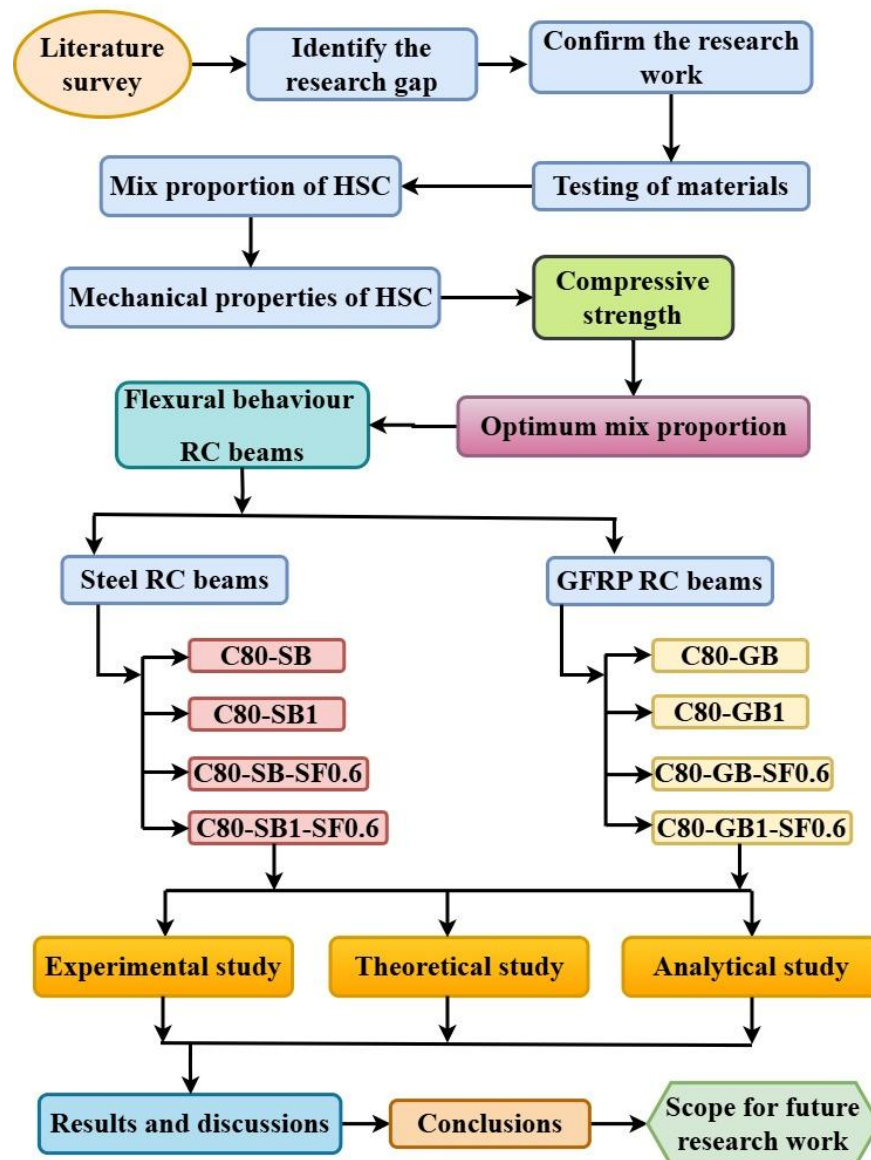


Figure 1. Research methodology of this study.

This study evaluated the flexural behaviour of RC beams reinforced with GFRP and steel rebar using high-strength concrete. A total of 8 RC beams (C80-SB, C80-GB, C80-SB1, C80-GB1, C80-SB-SF0.6, C80-GB-SF0.6, C80-SB1-SF0.6, and C80-GB1-SF0.6) were examined under two-point loading. Additionally, the flexural behaviour of RC beams (C80-SB, C80-GB, C80-SB1, and C80-GB1) was studied with the inclusion of 0.6% steel fibre (C80-SB-SF0.6, C80-GB-SF0.6, C80-SB1-SF0.6, and C80-GB1-SF0.6). Adding 0.6% steel fibre enhanced the flexural behaviour of the RC beams. GFRP RC beams exhibited superior flexural performance compared to steel RC beams. Furthermore, increasing the steel percentage in RC beams (C80-SB1 and C80-GB1) improved load-carrying capacity, ductility, stiffness, and energy absorption capacity compared to control RC beams (C80-SB and C80-GB). The main objective of this study was to enhance the load-carrying capacity, ductility, stiffness, energy absorption capacity, absorption ductility, mode of failure, and cracking pattern of the investigated RC beams. The research methodologies of this study are depicted in Figure 1.

2. Experimental program

2.1. Materials properties

The present study examined HSC beams reinforced with steel and GFRP rebar. The mix proportion for the high-strength concrete was designed in accordance with Indian Standard (IS: 10262 – 2019), as reported in Table 1. The concrete mixes included OPC 53 grade, confirming (IS: 12269 – 1987), silica fume, fly ash as fine aggregate, confirming (IS: 383 – 2016), coarse aggregate, confirming (IS: 383 – 2016), and superplasticizer. Additionally, 0.6% hook-end steel fibres were added to the HSC mix. The compressive strength was determined at 28 days, resulting in 81.64 MPa for C80-SB and 83.42 MPa for C80-SB-SF0.6. This study investigated reinforced concrete beams using two different concrete mixes. The OPC 53 grade cement is commonly used for high-strength concrete due to its superior performance. Silica fume, an ultrafine material, enhances the mechanical properties of concrete. When used as an acceptable aggregate replacement, fly ash can improve strength and durability. Combining these materials enhances the overall performance of high-strength concrete.

Table 1. Mix proportion of the high-strength concrete per 1m³.

Mix ID	Cement (kg/m ³)	Silica fume (kg/m ³)	Fly ash (kg/m ³)	FA (kg/m ³)	CA (kg/m ³)	WC (kg/m ³)	SP (kg/m ³)	W/B	SF (%)	CS (MPa)
C80-SB	440	44	22	658	1064	124	2.51	0.26	0	81.64
C80-SB-SF0.6	440	44	22	658	1064	124	2.51	0.26	0.6	83.42

Note: FA: fine aggregate, CA: coarse aggregate, WC: water content, SP: superplasticizer, W/B: water binding ratio, SF: steel fibre, CS: compressive strength.

2.2. Steel and GFRP rebars

This study used steel and GFRP rebar diameters of 8mm, 10mm, and 12mm to investigate the Reinforced Concrete (RC) beams, as shown in Figure 2. The GFRP bars were bought from Viruksha Composite in Andhra Pradesh. Specifically, the 8mm diameter rebar was employed in the compression zone, while the 10mm and 12mm diameters were utilized in the tension zone. The tensile strength of both the steel and GFRP rebars was determined, and their mechanical properties were evaluated according to (IS 1786-2008) and (ASTM D7205-2022), as detailed in Table 2. Additionally, the stress-strain curve for each rebar is depicted in Figure 3.

Table 2. Mechanical properties of the rebars.

Properties	Steel rebar			GFRP rebar		
	8mm	10mm	12mm	8mm	10mm	12mm
Ultimate stress (MPa)	475.62	482.84	485.32	768.14	892.67	974.73
Young's modulus (GPa)	200	201	200	38	38	39
Strain (mm/mm)	0.0019	0.0021	0.0022	0.0026	0.0024	0.0021

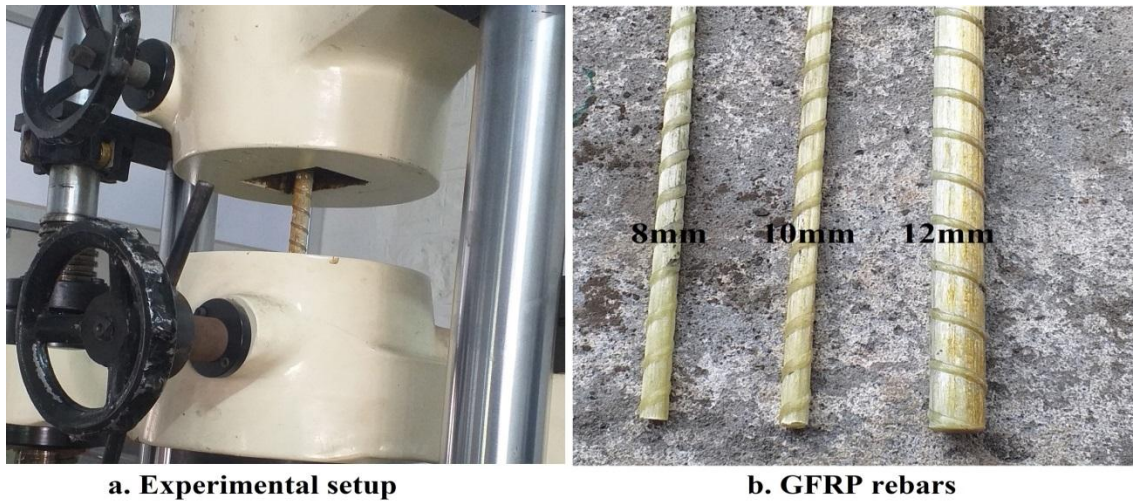


Figure 2. Experimental setup of GFRP rebars.

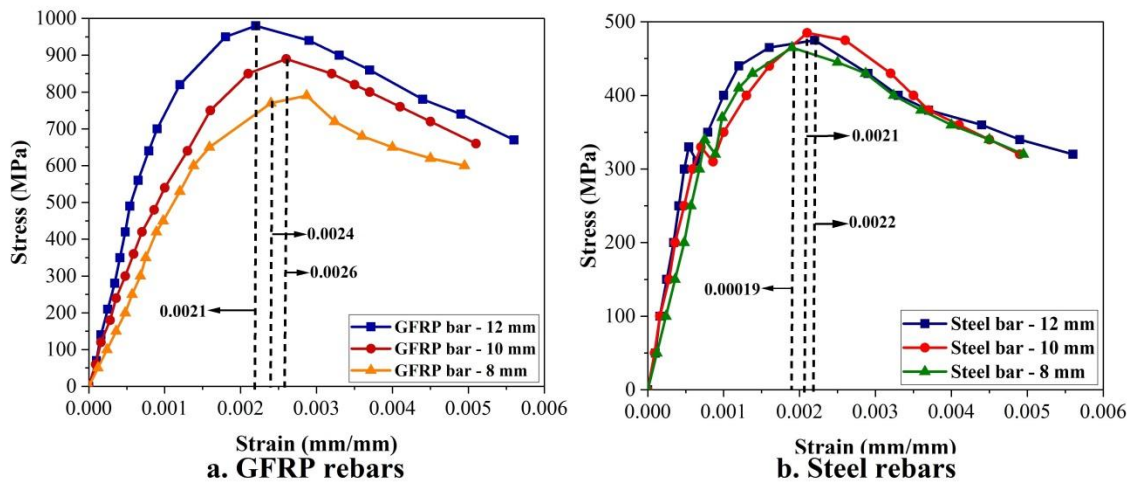


Figure 3. Stress-strain curve for GFRP and steel rebar.

2.3. Fabrication of specimens

The RC beams were fabricated with and without steel fibre. The reinforcement beam dimensions were 150 mm x 200 mm, with a length of 2500 mm. Additionally, the reinforced concrete beam was divided into two groups. Each group had four RC beams using steel and GFRP rebars, specifically (C80-SB, C80-SB1, C80-SB-SF0.6, C80-SB1-SF0.6) and (C80-GB, C80-GB1, C80-GB-SF0.6, C80-GB1-SF0.6). These details are presented in Table 3. In total, 8 RC beams were fabricated and designed according to (IS: 456 - 2000). The cross-sectional and longitudinal reinforcement details of the RC beams are shown in Figures 4 and 5, respectively. The steel cage was placed on the steel mould with proper alignment, and a high-strength concrete mix was poured into the steel mould and compacted using a vibrator. The excess concrete was then removed and levelled. The steel mould was left at room temperature for 24 hours. Subsequently, the RC beam was carefully removed from the steel mould without damage and placed in a water tank for 28 days of curing.

Table 3. Geometric details of the specimens.

Group	Specimen ID	Dimension (BXDXL)	Bottom	Top	Shear reinforcement
I	C80-SB	150mm x 200mm x 2500mm	2#12mm	2#8mm	#6mm @ 100mm c/c
	C80-GB	150mm x 200mm x 2500mm	2#12mm	2#8mm	#6mm @ 100mm c/c
	C80-SB1	150mm x 200mm x 2500mm	2#12mm - 1#10mm	2#8mm	#6mm @ 100mm c/c
	C80-GB1	150mm x 200mm x 2500mm	2#12mm - 1#10mm	2#8mm	#6mm @ 100mm c/c
II	C80-SB-SF0.6	150mm x 200mm x 2500mm	2#12mm	2#8mm	#6mm @ 100mm c/c
	C80-GB-SF0.6	150mm x 200mm x 2500mm	2#12mm	2#8mm	#6mm @ 100mm c/c
	C80-SB1-SF0.6	150mm x 200mm x 2500mm	2#12mm - 1#10mm	2#8mm	#6mm @ 100mm c/c
	C80-GB1-SF0.6	150mm x 200mm x 2500mm	2#12mm - 1#10mm	2#8mm	#6mm @ 100mm c/c

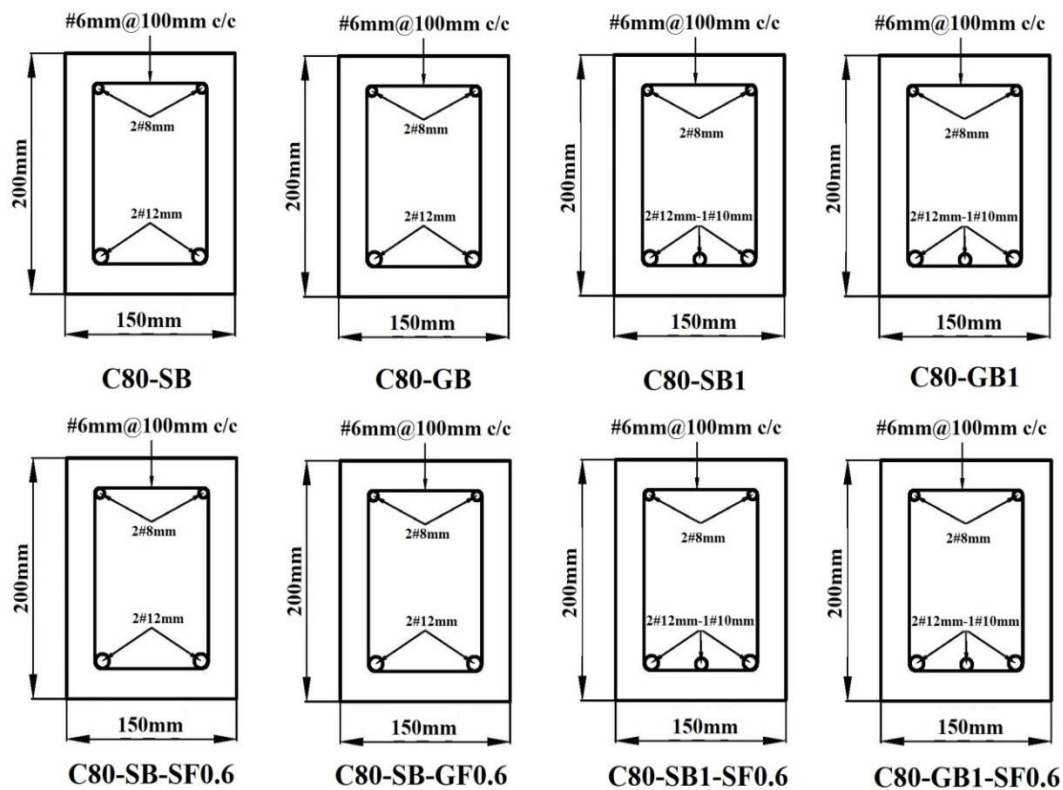


Figure 4. Cross-sectional details of all specimens.

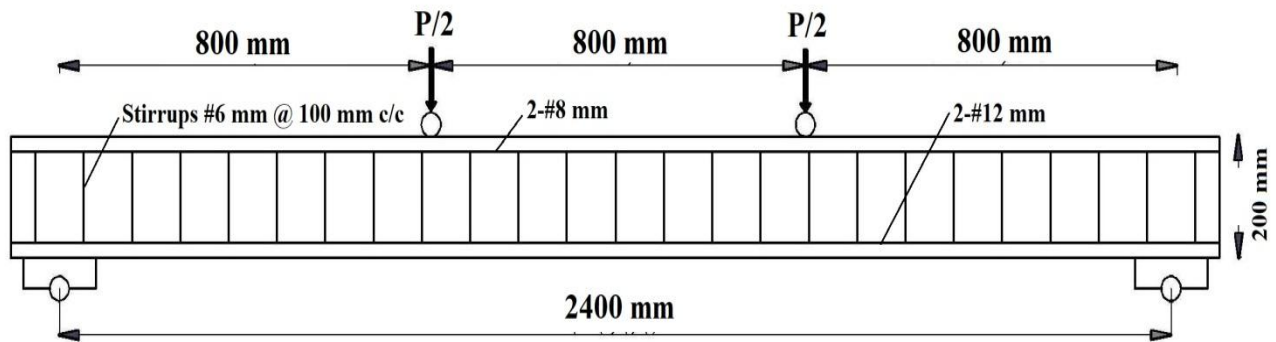


Figure 5. Longitudinal reinforcement details of the specimen.

2.4. Experimental setup of the specimens

The RC beams were removed from the curing tank, and their outer surfaces were cleaned. Concentrated two-point loading was applied to all RC beams, testing them under the 50T capacity of the loading frame. The experimental setup is shown in Figure 6. The RC beams were controlled in stress-control mode, with a loading rate of 0.5 mm/minute for all. Loading continued until the RC beams failed. During the experimental study, a deflection meter was placed under the beam at midspan and at $L/3$, and deflections were recorded. The initial and ultimate failure load and deflection were recorded for all RC beams.



Figure 6. Experimental setup of specimens.

3. Results and discussion

3.1. Load-deflection response of the RC beams

The deflection of all group specimens was measured, and the corresponding load-deflection curve is depicted in Figure 7. Figure 8 illustrates the ultimate load and deflection of all group specimens. Generally, the load-deflection curves are divided into three points: the first point represents concrete cracking, the second point corresponds to steel yielding, and the third point is considered the ultimate point, as shown in Figure 9. The ultimate point is when the specimens fail after reaching that critical stage. The load-deflection curve exhibits a linear behaviour during these three stages. Initially, cracks form in the specimen's tension zone during the first stage. Subsequently, the crack propagates throughout the specimen as a gradual load is applied in the second stage. Finally, in the third stage, the specimens fail at the ultimate point, either by concrete crushing

or shear failure. These three stages are commonly observed across all specimens (C80-SB, C80-GB, C80-SB-SF0.6, C80-GB-SF0.6, C80-SB1, C80-GB1, C80-SB1-SF0.6, and C80-GB1-SF0.6).

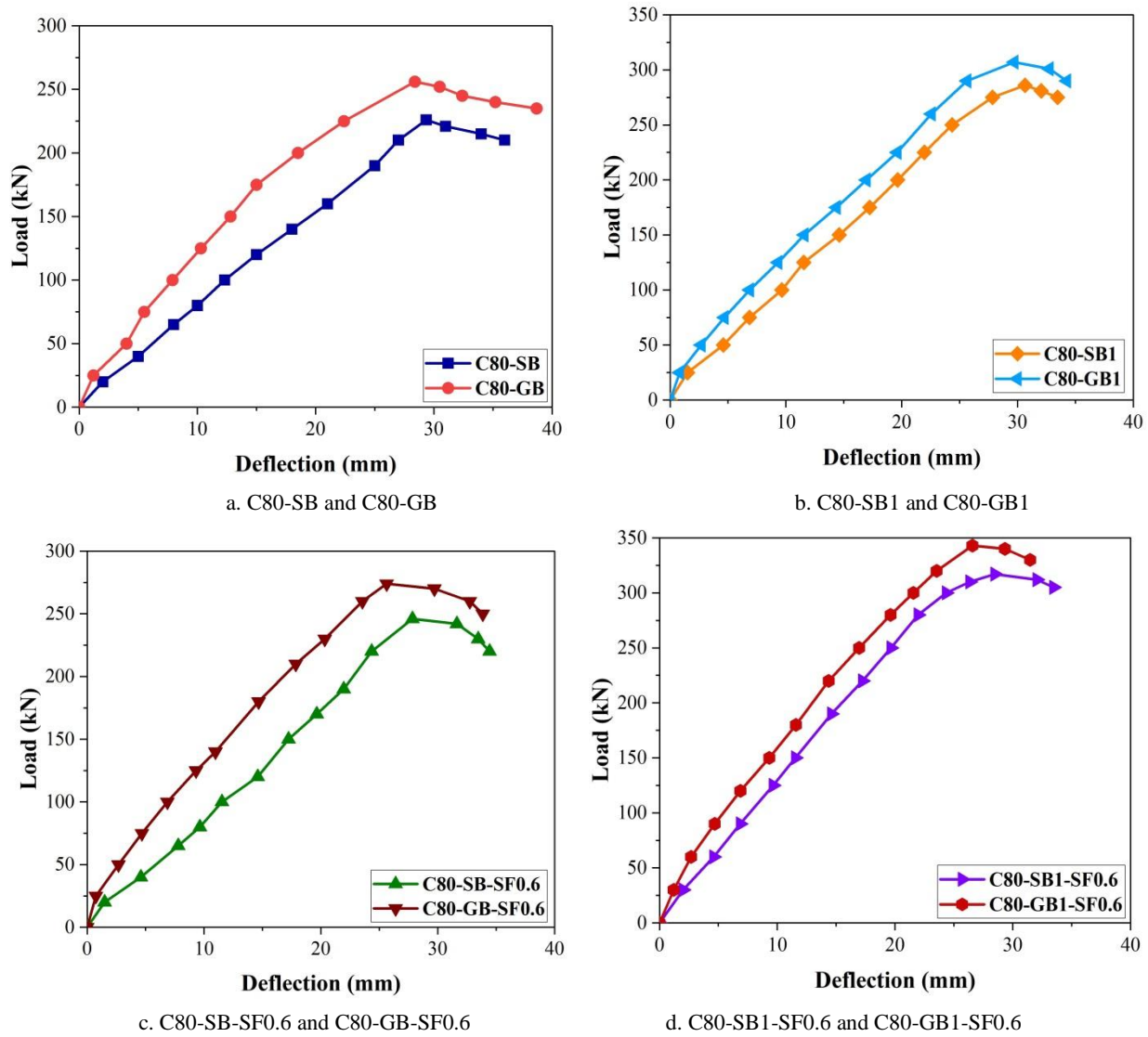


Figure 7. Load-deflection response of all group specimens.

The load-carrying capacity of steel and GFRP RC beams (C80-GB, C80-GB1) is compared. Notably, GFRP RC beams exhibit a higher load-carrying capacity than steel RC beams (C80-SB, C80-SB1). Furthermore, the addition of 0.6% steel fibres enhances the load-carrying capacity of both steel and GFRP RC beams (C80-GB-SF0.6, C80-GB1-SF0.6) compared to their counterparts without fibres (C80-SB-SF0.6, C80-SB1-SF0.6). The ultimate load-carrying capacity and deflection of all RC specimens were observed in the experimental study, with values as follows: 226.14 kN, 256.37 kN, 246.52 kN, 274.67 kN, 286.14 kN, 307.28 kN, 317.74 kN, and 343.18 kN for C80-SB, C80-GB, C80-SB1, C80-GB1, C80-SB-SF0.6, C80-GB-SF0.6, C80-SB1-SF0.6, and C80-GB1-SF0.6 specimens, respectively. The corresponding deflections were observed in 29.36 mm, 28.42 mm, 27.84 mm, 25.68 mm, 30.65 mm, 29.72 mm, 28.47 mm, and 26.58 mm.

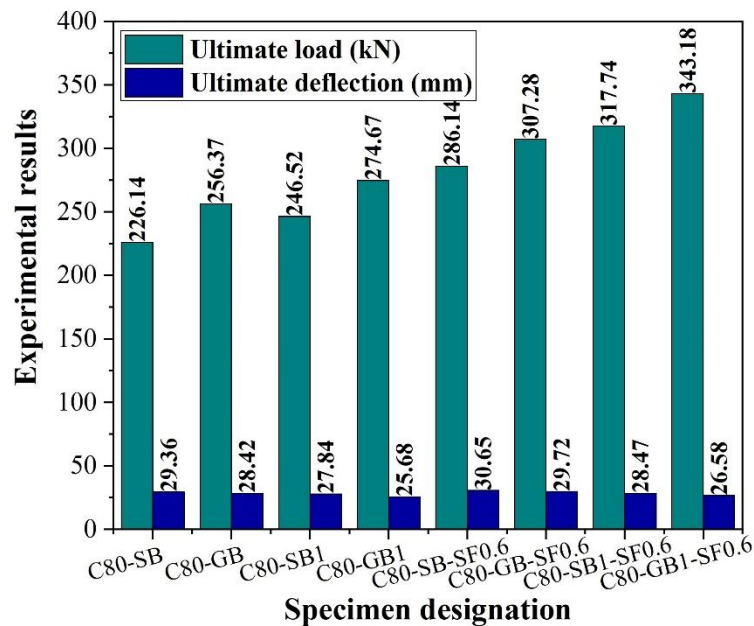


Figure 8. Ultimate load-deflection responses of all groups of specimens.

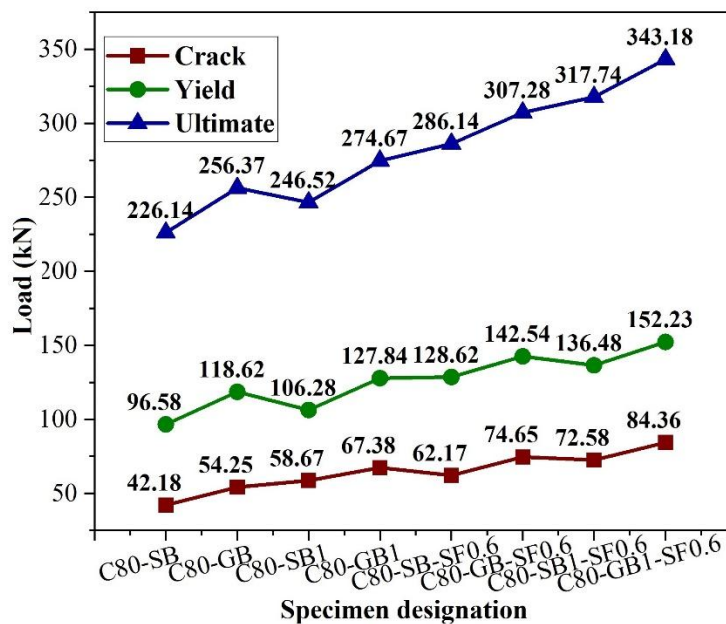


Figure 9. Concrete crack, yield and ultimate load of all specimens.

3.2. Failure mode

All tested RC beams in this study exhibited two standard failure modes, as presented in Table 4. The tested specimens are shown in Figure 10. Concrete crushing occurred in the RC beams (C80-SB, C80-GB, C80-GB1, C80-SB-SF0.6, C80-GB-SF0.6, and C80-GB1-SF0.6), while shear failure was observed in the RC beams (C80-SB1-SF0.6 and C80-SB1) during the experimental study. The addition of 0.6% steel fibre significantly enhanced the load-carrying capacity of the RC beams by 26.53%, 19.85%, 28.89%, and 24.94% for (C80-SB-SF0.6, C80-GB-SF0.6, C80-SB1-SF0.6, and C80-GB1-SF0.6) compared to the control RC beams (C80-SB, C80-GB, C80-SB1, and C80-GB1). Additionally, GFRP RC beams exhibited improved

load-carrying capacity by 13.37% and 11.42% for (C80-GB and C80-GB1) compared to the steel RC beams (C80-SB and C80-SB1). Including 0.6% steel fibre, they enhanced the flexural behaviour of the RC beams and reduced crack width in the specimens. Notably, more cracks were observed in the compression and tension zones. Shear and flexural cracks were also evident in all RC specimens. As the load approached the yield point, it gradually increased, leading to the propagation of shear and flexural cracks throughout the RC specimens.

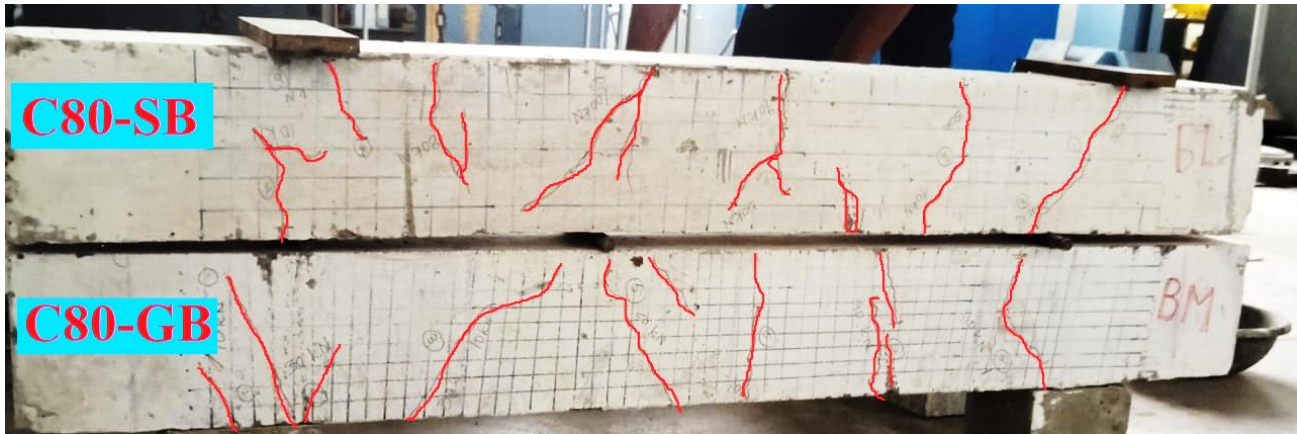


Figure 10. Tested specimens.

Table 4. Experimental load, ductility and stiffness of the specimens.

Specimen ID	Load (kN)			Deflection (mm)			Ductility		Stiffness (kN/mm)		E _u (J)	Mode of failure
	P _Y	P _U	P _F	Yield	Ultimate	Failure	Yield	Ultimate	Yield	Ultimate		
C80-SB	96.58	226.14	221.67	12.37	29.36	30.82	2.37	1.05	7.81	7.70	5240.79	CC
C80-GB	118.62	256.37	252.43	10.48	28.42	31.57	2.71	1.11	11.32	9.02	5942.66	CC
C80-SB1	106.28	246.52	242.38	13.67	27.84	31.65	2.04	1.14	7.77	8.85	5178.15	SF
C80-GB1	127.84	274.67	270.94	11.32	25.68	29.72	2.27	1.16	11.29	10.70	5498.89	CC
C80-SB-SF0.6	128.62	286.14	281.37	11.54	30.65	32.06	2.66	1.05	11.15	9.34	7119.16	CC
C80-GB-SF0.6	142.54	307.28	301.62	9.32	29.72	32.75	3.19	1.10	15.29	10.34	7700.44	CC
C80-SB1-SF0.6	136.48	317.74	312.42	11.54	28.47	32.06	2.47	1.13	11.83	11.16	7212.70	SF
C80-GB1-SF0.6	152.23	343.18	340.37	9.32	26.58	31.84	2.85	1.20	16.33	12.91	7522.51	CC

Note: P_Y – yield load; P_U – ultimate load; P_F – failure load; E – energy absorption, CC – concrete crushing, SF – shear failure

3.3. Ductility and energy absorption capacity

The ductility index was examined in this study, defined as the ratio of the ultimate deflection (Δ_u) to the yield deflection (Δ_y) of the RC beams. The RC beams were divided into three stages, as illustrated in Figure 11. In the first stage, the specimens exhibited a linear load-deflection curve up to the yield point. Minor cracks formed in this stage, denoted as (Δ_y). In the second stage, the load was gradually increased, resulting in shear and flexural cracks throughout the specimens. In this stage, the specimens partially failed, and the elastic-to-plastic limit was reached, denoted as (Δ_u). Finally, in the third stage, the specimens failed at the ultimate load (Δ_f). The yield and ultimate ductility indices were determined using Equations (1) and (2), as displayed in Figure 12.

$$\text{Ductility index } (\mu_y) = \left(\frac{\Delta_u}{\Delta_y} \right) \quad (1)$$

$$\text{Ductility index } (\mu_u) = \left(\frac{\Delta_f}{\Delta_u} \right) \quad (2)$$

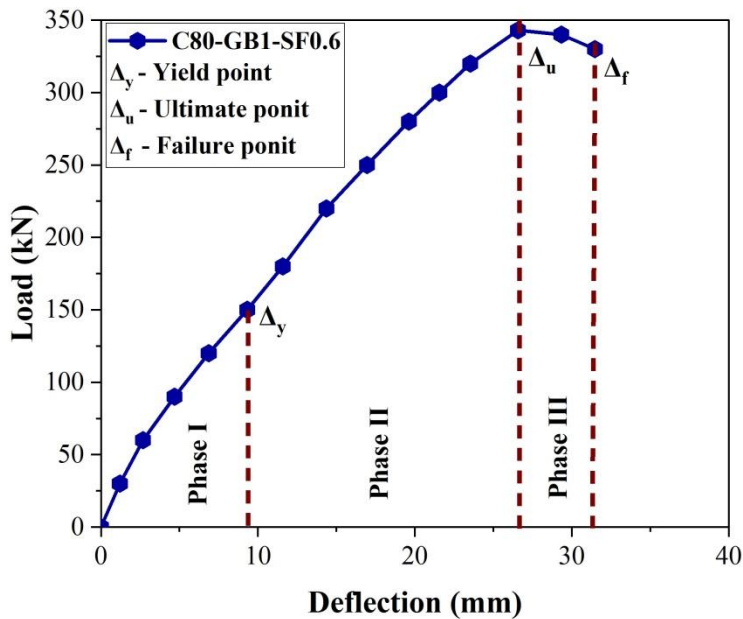


Figure 11. Ductility index calculation of the specimen.

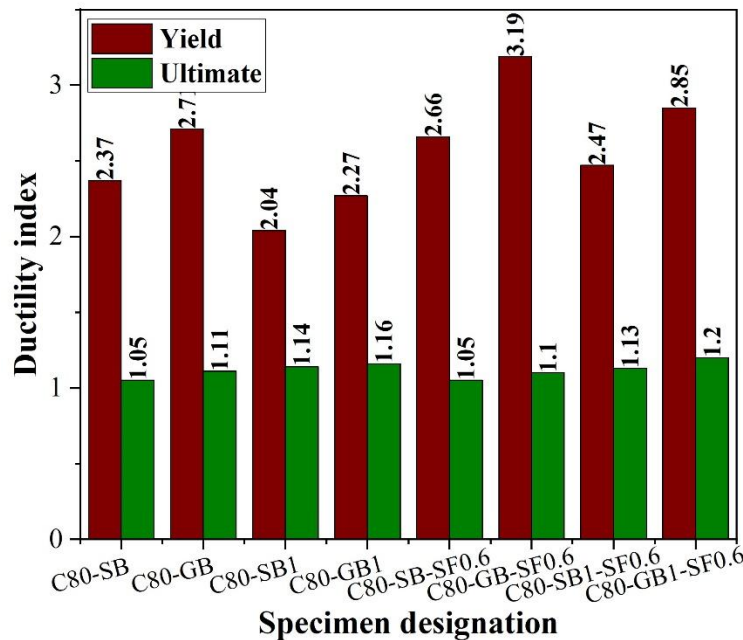


Figure 12. Ductility index of all groups of specimens.

The energy absorption capacity (E) of the RC beams was determined based on the area enclosed by the load-deflection curve, as depicted in Figure 13. The total energy absorption capacity ($E = E_y + E_u$) was calculated, including the yield energy absorption capacity (E_y) and the ultimate energy absorption capacity (E_u) of the RC beams, as shown in Figure 14. The energy absorption capacity coefficient (E_u / E_y) was examined for all RC beams, as illustrated in Figure 15. The maximum energy ductility coefficient was observed in the C80-SB-SF0.6 and C80-SB1-SF0.6 specimens. Specifically, the steel RC beams exhibited a high energy ductility coefficient of 10.65 for C80-SB-SF0.6, while the steel RC beam had a high energy ductility of 8.55 for C80-SB1-SF0.6. Additionally, stiffness was determined for all RC beams, as represented in Figure 16.

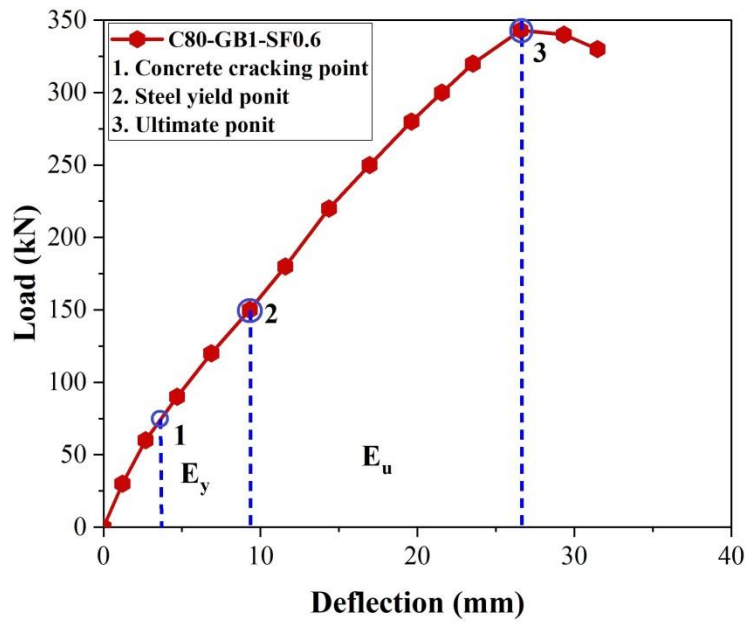


Figure 13. Energy absorption calculation of the specimen.

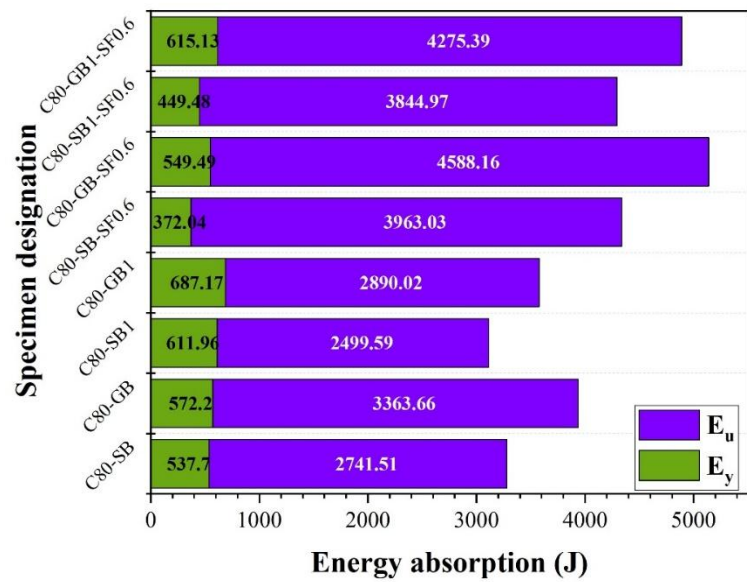


Figure 14. Yield and ultimate energy absorption of all group specimens.

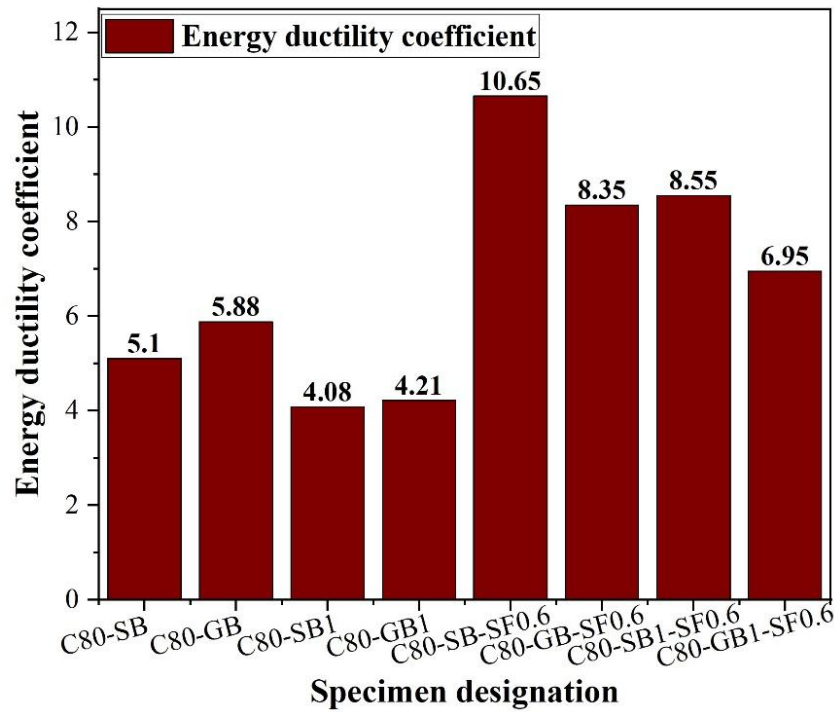


Figure 15. Energy ductility coefficient of all group specimens.

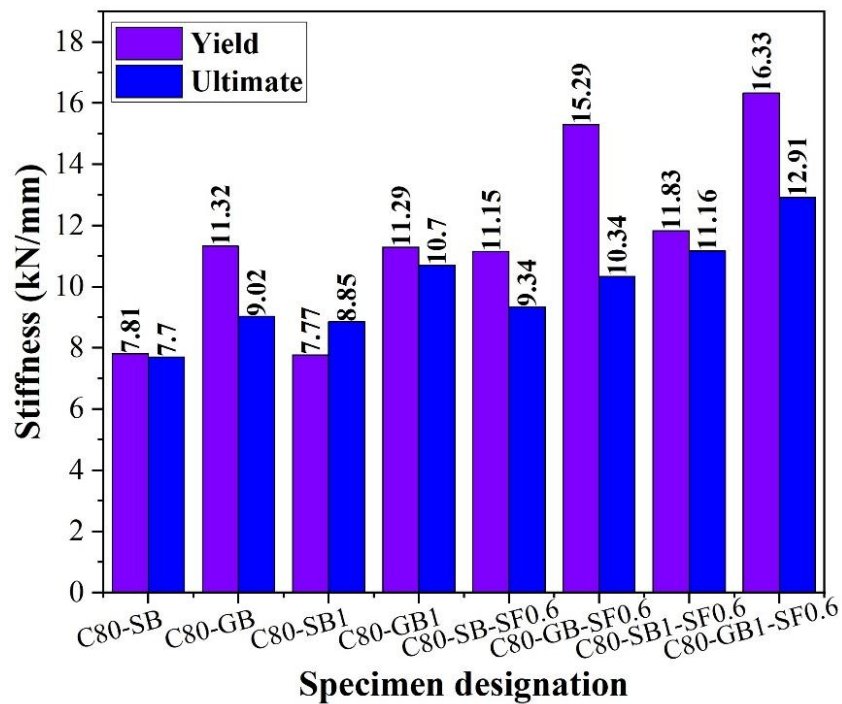


Figure 16. Yield and ultimate stiffness of all specimens.

4. Analytical study

4.1. Current design-code approach to deflection calculation.

Initially, the effective moment of inertia is computed using Branson's method equation (3). Branson's method was modified based on experimental findings to account for the effect of moment of inertia (ACI 440.1R-06). Reduction coefficients, bond characteristics, and the modulus of elasticity of the GFRP rebar are all included in the improved equation (4) (CSA S806-02).

$$I_e = I_g \left(\frac{M_{cr}}{M_a} \right)^3 + I_{cr} \left(1 - \left(\frac{M_{cr}}{M_a} \right)^3 \right) \leq I_g \quad (3)$$

$$\beta_d = \frac{1}{5} \left(\frac{\rho_f}{\rho_{fb}} \right) \leq 1.0 \quad (4)$$

Where: $M_{cr} = \left(\frac{f_r}{f_{rb}} \right)$, $f_r = 0.6 \sqrt{f'_c}$

In this case, I_e represents the effective moment of inertia, I_g denotes the gross section effective moment of inertia, and I_{cr} is the effective moment of inertia that cracks the transferred concrete area. Concrete modulus of rupture, cracking moment, service moment, and compressive strength are denoted by the letters M_{cr} , M_a , f'_c , and f_r .

4.2. Proposed method for the prediction of deflection

Using the previously derived equations, both the practical and theoretical moment of inertia are computed in Equations (5) and (6). The modification factor β_d was determined based on a balanced and actual ratio. Experimental load-deflection data were utilized to calculate the coefficients X_1 and X_2 .

$$(I_c)_{exp} = \frac{P_{exp} L_a}{48 E_c \delta_{exp}} (3L^2 - 4L_a^2) \quad (5)$$

$$(I_e)_{Theo} = \beta_d \left(\frac{M_{cr}}{M_a} \right)^3 I_g + X_2 \left(1 - \left(\frac{M_{cr}}{M_a} \right)^3 \right) I_{cr} \leq I_g \quad (6)$$

$$\beta_d = X_1 \left(\frac{\rho_f}{\rho_{fb}} \right) \leq 1.0$$

where L and L_a are the total and effective lengths of the specimen, δ is the mid-span deflection of the specimens, and E_c is the concrete's modulus of elasticity. The terms actual and balanced reinforcement ratios refer to ρ_f and ρ_{fb} , respectively. The modification factor is β_d .

4.3. Evaluate the proposed method for the prediction of deflection.

The proposed approaches (ACI 440.1R and CSA S806-02) were compared with the experimental results presented in Table 5. Equations (5) and (6) were used to obtain the practical and theoretical moment of inertia. The experimental mid-span deflection, with a mean of 0.99, a standard deviation of 0.01, and a coefficient of variation of 1.12%, agreed with the proposed methods. Both (CSA S806-02) and (ACI 440.1R) predicted the mid-span deflection. They have mean values of 1.03 and 1.01. The coefficient of variation is 1.70% and 2.50%, while the standard deviation is 0.02 and 0.03, respectively. Figures 17 and 18 show the 10% observed deviation from the predicted mid-span deflection, as determined by the experimental codes.

Table 5. Comparative study between experiment and predicted deflection for all specimens.

Specimen ID	Experiment deflection (mm)	Proposed method		CSA S806		ACI 440.1 R	
		δ_{Pred}	$\delta_{Exp}/\delta_{Pred}$	δ_{Pred}	$\delta_{Exp}/\delta_{Pred}$	δ_{Pred}	$\delta_{Exp}/\delta_{Pred}$
C80-SB	29.36	29.78	0.99	29.08	1.01	28.42	1.03
C80-GB	28.42	28.14	1.01	27.54	1.03	27.96	1.02
C80-SB1	27.84	27.68	1.01	28.06	0.99	27.32	1.02
C80-GB1	25.68	25.86	0.99	26.42	0.97	24.67	1.04
C80-SB-SF0.6	30.65	31.08	0.99	29.87	1.03	28.92	1.06
C80-GB-SF0.6	29.72	30.47	0.98	28.62	1.04	29.47	1.01

C80-SB1-SF0.6	28.47	28.69	0.99	28.96	0.98	27.84	1.02
C80-GB1-SF0.6	26.58	26.74	0.99	25.79	1.03	25.37	1.05
Mean	-	-	0.99	-	1.01	-	1.03
SD	-	-	0.01	-	0.03	-	0.02
COV (%)	-	-	1.12	-	2.50	-	1.70

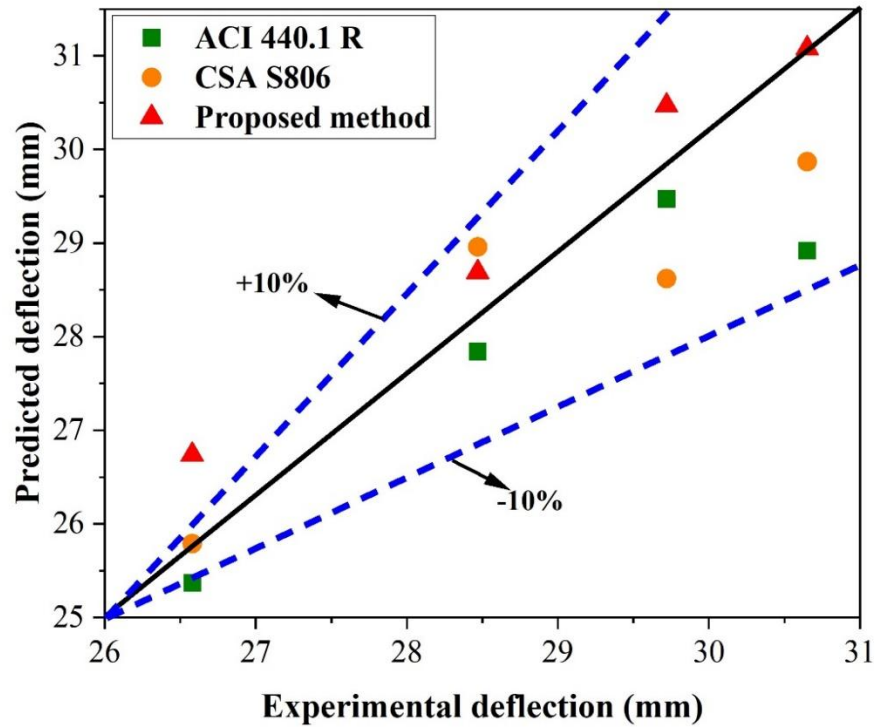


Figure 17. Evaluate the deflection of all specimens for experimental codes and the proposed method.

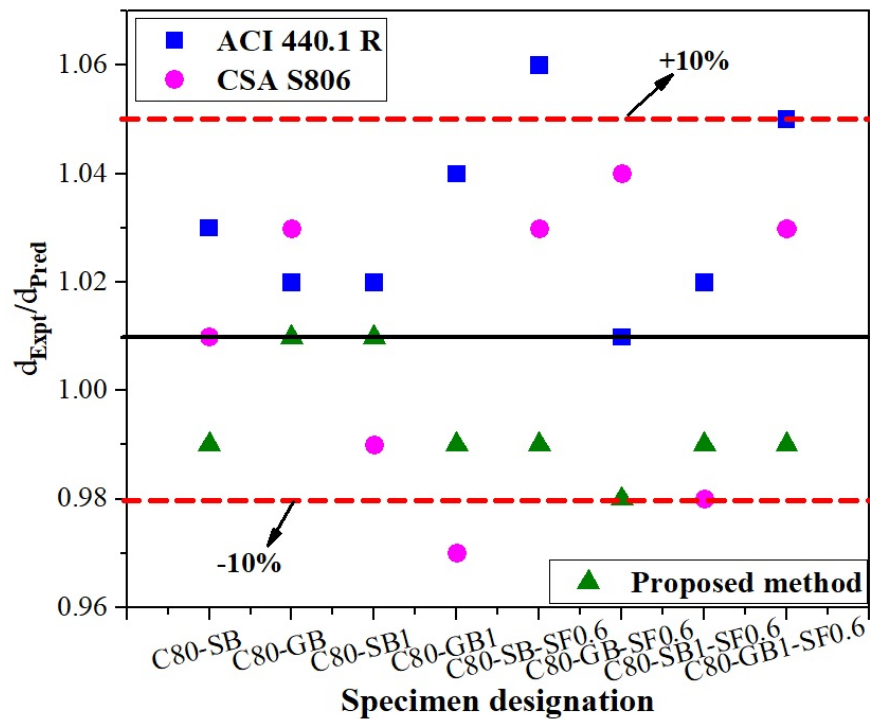


Figure 18. Ratio between the experimental and the proposed method results of all specimens.

5. Conclusions

The present study investigates the flexural behaviour of GFRP and steel RC beams under two-point loading. A total of 8 beams were studied, including two GFRP RC beams, C80-GB and C80-GB1; Two steel RC beams, C80-GB and C80-GB1; Two GFRP RC beams with 0.6% steel fibre: C80-GB-SF0.6 and C80-GB1-SF0.6; Two GFRP RC beams without steel fibre: C80-GB-SF0.6 and C80-GB1-SF0.6. The GFRP RC beams outperformed the steel RC beams. The experimental study led to the following conclusions:

1. The load-carrying capacity of GFRP RC beams was superior to that of steel RC beams. Concrete crushing failure was commonly observed in all specimens.
2. More flexural and shear cracks were observed in the GFRP RC beams, and the load-deflection curve of GFRP and steel RC beams exhibited similar behaviour.
3. Replacing steel rebar with GFRP rebar improved the load-carrying capacity, ductility, and stiffness of RC beams. Additionally, the energy absorption capacity of GFRP RC beams exceeded that of steel RC beams.
4. Adding 0.6% steel fibre further enhanced the overall performance of both steel and GFRP RC beams, including load-carrying capacity, ductility, stiffness, and energy absorption. The energy ductility coefficient was excellent for C80-SB-SF0.6 and C80-SB1-SF0.6. Moreover, the steel fibres prevented shear and flexural cracks.
5. Increasing the steel and GFRP ratios improved load-carrying capacity, ductility, and stiffness compared with the control specimens.
6. The mid-span deflection of the RC specimens was determined using the proposed method, and the mid-span deflection of the specimens was predicted using CSA S806 codes and ACI 440.1R codes. The proposed methods agree with the experimental test outcomes based on the analytical analysis. The specimens' respective means, standard deviations, and coefficients of variation are 0.99, 0.01, and 1.12%.

Future research may explore the following areas:

1. The impact of different GFRP ratios, varying fibre contents, and alternative fibre types on flexural and shear performance to determine optimal reinforcement combinations.
2. The durability, fatigue resistance, and serviceability of GFRP and hybrid RC beams when subjected to sustained loads, cyclic loading, and harsh environmental conditions.
3. Creating sophisticated predictive models and validating them with extensive experimental data will improve the precision of predictions for deflection, crack propagation, and energy absorption in real-world design applications.

Author contributions: Sasikumar P: Participated in planning for the study, design, analytical, experimental parametric study, research methodology, implementation of the parametric study, and writing original manuscript preparation, reviewing the manuscript and supervising experimental works.

Funding: No funding agency has supported this project.

Acknowledgements: The authors gratefully acknowledge the K.Ramakrishnan College of Technology for providing all the required facilities to accomplish this study.

Conflicts of interest: The authors declare no conflicts of interest.

References

- Abdalla, H.A. (2002). Evaluation of deflection in concrete members reinforced with fibre reinforced polymer (FRP) bars. *Composite Structures*, 56(1), 63-71.
- Abdallah, M., Al Mahmoud, F., Khelil, A., Mercier, J., and Almassri, B. (2020). Assessment of the flexural behaviour of continuous RC beams strengthened with NSM-FRP bars, experimental and analytical study. *Composite Structures*, 242, 112127.
- ACI Committee 440. ACI 440.1R-06, Guide for the design and construction of concrete reinforced with FRP bars. Farmington Hills, Mich., USA: American Concrete Institute.
- Adam, M.A., Said, M., Mahmoud, A.A., and Shanour, A.S. (2015). Analytical and experimental flexural behaviour of concrete beams reinforced with glass fibre reinforced polymers bars. *Construction and building materials*, 84, 354-366.
- Ahmed, H.Q., Jaf, D.K., and Yaseen, S.A. (2020). Flexural capacity and behaviour of geopolymers concrete beams reinforced with glass fibre-reinforced polymer bars. *International Journal of Concrete Structures and Materials*, 14(1), 14.
- Alsayed, S.H., Al-Salloum, Y.A., and Almusallam, T.H. (2000). Performance of glass fibre reinforced plastic bars as a reinforcing material for concrete structures. *Composites Part B: Engineering*, 31(7), 555-567.
- ASTM D7205-2022 Standard Test Method for Tensile Properties of Fibre Reinforced Polymer Matrix Composite Bars.
- Aydin, F. (2019). Experimental study on the flexural behaviour of a novel concrete filled hybrid beams reinforced with GFRP and steel bars. *KSCE Journal of Civil Engineering*, 23(11), 4710-4717.
- CAN, CSA S806-02. Design and construction of building components with fibre reinforced polymers. Canadian Standards Association.
- Cao, S., Wu, C., and Wang, W. (2020). Behaviour of FRP confined UHPFRC-filled steel tube columns under axial compressive loading. *Journal of Building Engineering*, 32, 101511.
- Carrillo, J., Araya-Letelier, G., and Tarque, N. (2025). Shear stress and angular strain prediction of concrete panels reinforced with GFRP bars. *Engineering Structures*, 327, 119610.
- Chaallal, O., and Benmokrane, B. (1996). Fibre-reinforced plastic rebars for concrete applications. *Composites Part B: Engineering*, 27(3), 245-252.
- El-Nemr, A., Ahmed, E.A., El-Safty, A., and Benmokrane, B. (2018). Evaluation of the flexural strength and serviceability of concrete beams reinforced with different types of GFRP bars. *Engineering Structures*, 173, 606-619.
- Ferdous, W., Manalo, A., AlAjarmeh, O., Mohammed, A.A., Salih, C., Yu, P., Khotbehsara, M.M., and Schubel, P. (2021). Static behaviour of glass fibre reinforced novel composite sleepers for mainline railway track. *Engineering Structures*, 229, 111627.
- Ge, W., Han, M., Guan, Z., Zhang, P., Ashour, A., Li, W., Lu, W., Cao, D., and Yao, S. (2021). Tension and bonding behaviour of steel-FRP composite bars subjected to the coupling effects of chloride corrosion and load. *Construction and Building Materials*, 296, 123641.

- Ge, W., Song, W., Ashour, A.F., Lu, W., and Cao, D. (2020). Flexural performance of FRP/steel hybrid reinforced engineered cementitious composite beams. *Journal of Building Engineering*, 31, 101329.
- Goldston, M.W., Remennikov, A., and Sheikh, M.N. (2017). Flexural behaviour of GFRP reinforced high strength and ultra-high strength concrete beams. *Construction and Building Materials*, 131, 606-617.
- Guo, F., Al-Saadi, S., Raman, R.S., and Zhao, X.L. (2018). Durability of fibre reinforced polymer (FRP) in simulated seawater sea sand concrete (SWSSC) environment. *Corrosion Science*, 141, 1-13.
- Guo, Y.C., Xiao, S.H., Shi, S.W., Zeng, J.J., Wang, W.Q., and Zhao, H.C. (2020). Axial compressive behaviour of concrete-filled FRP-steel wire reinforced thermoplastics pipe hybrid columns. *Composite Structures*, 244, 112237.
- Guo, Y.C., Ye, Y.Y., Lv, J.F., Bai, Y.L., and Zeng, J.J. (2020a). Effective usage of high-strength steel tubes: Axial compressive behaviour of hybrid FRP-concrete-steel solid columns. *Thin-Walled Structures*, 154, 106796.
- Hadi, M.N., Hasan, H.A., and Sheikh, M.N. (2017). Experimental investigation of circular high-strength concrete columns reinforced with glass fibre-reinforced polymer bars and helices under different loading conditions. *Journal of Composites for Construction*, 21(4), 04017005.
- Hasan, H.A., Sheikh, M.N., and Hadi, M.N. (2018). Analytical investigation on the load-moment characteristics of GFRP bar reinforced circular NSC and HSC columns. *Construction and Building Materials*, 183, 605-617.
- IS 10262 – 2019. Guidelines for concrete mix design proportioning. Bureau of Indian standards, New Delhi.
- IS 12269 – 1987. Specification for 53 grade ordinary Portland cement. Bureau of Indian standards, New Delhi
- IS 1786 - 2008. Specification for high-strength deformed steel bars and wires for concrete reinforcement. Indian Standard, New Delhi.
- IS 383 – 2016. Specification for coarse and fine aggregate from natural sources for concrete. Bureau of Indian standards, New Delhi.
- IS 456 - 2000. Plain and Reinforced Concrete - Code of Practice. Indian Standard, New Delhi.
- Junaid, M.T., Elbana, A., Altoubat, S., and Al-Sadoon, Z. (2019). Experimental study on the effect of matrix on the flexural behaviour of beams reinforced with Glass Fibre Reinforced Polymer (GFRP) bars. *Composite Structures*, 222, 110930.
- Lau, D., and Pam, H.J. (2010). Experimental study of hybrid FRP reinforced concrete beams. *Engineering Structures*, 32(12), 3857-3865.
- Liu, S., Zhou, Y., Zhou, J., Zhang, B., Jin, F., Zheng, Q., and Fan, H. (2019). Blast responses of concrete beams reinforced with GFRP bars: Experimental research and equivalent static analysis. *Composite Structures*, 226, 111271.
- Manalo, A.C., Aravinthan, T., Karunasena, W., and Ticoalu, A. (2010). A review on alternative materials for replacement railway sleepers. *Compos. Struct.*, 92, 603-611.
- Nakano, K., Matsuzaki, Y., Fukuyama, H., and Teshigawara, M. (1993). Flexural performance of concrete beams reinforced with continuous fibre bars. *Special Publication*, 138, 743-766.
- Nanni, A., De Luca, A., and Zadeh, H.J. (2014). Reinforced concrete with FRP bars: Mechanics and design.
- Prakash, A., Priyadarshani, S.A., and Rao, S.V. (2025). Durability and structural integrity of columns reinforced with various combinations of steel and GFRP bars. *Case Studies in Construction Materials*, 23, e05017.
- Qu, W., Zhang, X., and Huang, H. (2009). Flexural behaviour of concrete beams reinforced with hybrid (GFRP and steel) bars. *Journal of Composites for construction*, 13(5), 350-359.
- Raza, A., Manalo, A.C., Rafique, U., and AlAjarmeh, O.S. (2021). Concentrically loaded recycled aggregate geopolymer concrete columns reinforced with GFRP bars and spirals. *Composite Structures*, 268, 113968.
- Saleh, Z., Goldston, M., Remennikov, A.M., and Sheikh, M.N. (2019). Flexural design of GFRP bar reinforced concrete beams: An appraisal of code recommendations. *Journal of Building Engineering*, 25, 100794.
- Salih, C., Manalo, A., Ferdous, W., Abousnina, R., Yu, P., Heyer, T., and Schubel, P. (2021). Novel bending test method for polymer railway sleeper materials. *Polymers*, 13(9), 1359.
- Sasikumar, P., and Manju, R. (2022). Structural behaviour of high strength concrete columns reinforced with glass fibre reinforced polymer bars under axial loading. *Revista Romana de Materiale*, 52(4), 412-423.
- Sasikumar, P., and Manju, R. (2023). Structural behaviour of axially loaded high strength concrete columns reinforced longitudinally with glass fibre reinforced polymer bars. *Revista de la construcción*, 22(2), 293-305.
- Sasikumar, P., and Manju, R. (2024). Flexural behaviour of reinforced concrete beams reinforced with Glass Fibre Reinforced Polymer (GFRP) bars: experimental and analytical study. *Asian Journal of Civil Engineering*, 25(2), 1-14.
- Schutte, C.L. (1994). Environmental durability of glass-fibre composites. *Materials Science and Engineering: Reports*, 13(7), 265-323.

- Sidhardhan, J.S., and Madaswamy, M. (2025). The structural performance of beam reinforced with steel bars and glass fibre reinforced polymer bars subjected to static and static cyclic loads. *Revista de la construcción*, 24(1), 100-117.
- Sun, Z.Y., Yang, Y., Qin, W.H., Ren, S.T., and Wu, G. (2012). Experimental study on flexural behaviour of concrete beams reinforced by steel-fibre reinforced polymer composite bars. *Journal of Reinforced Plastics and Composites*, 31(24), 1737-1745.
- Tavakol, M., and Kazemi, H.H. (2025). Comparative assessment of concrete columns reinforced with hybrid steel-GFRP, GFRP, and steel bars under cyclic lateral loading. In *Structures*, 71, 108034.
- Toutanji, H.A., and Saafi, M. (2000). Flexural behaviour of concrete beams reinforced with glass fibre-reinforced polymer (GFRP) bars. *Structural Journal*, 97(5), 712-719.
- Wang, H., and Belarbi, A. (2011). Ductility characteristics of fibre-reinforced-concrete beams reinforced with FRP rebars. *Construction and Building Materials*, 25(5), 2391-2401.
- Ye, Y.Y., Smith, S.T., Zeng, J.J., Zhuge, Y., and Quach, W.M. (2021). Novel ultra-high-performance concrete composite plates reinforced with FRP grid: Development and mechanical behaviour. *Composite Structures*, 269, 114033.
- Zeng, J.J., Chen, S.P., Zhuge, Y., Gao, W.Y., Duan, Z.J., and Guo, Y.C. (2021). Three-dimensional finite element modeling and theoretical analysis of concrete confined with FRP rings. *Engineering Structures*, 234, 111966.
- Zeng, J.J., Zheng, Y.W., Liu, F., Guo, Y.C., and Hou, C., (2021a). Behaviour of FRP Ring-Confined CFST columns under axial compression. *Composite Structures*, 257.



Copyright (c) 2026 Sasikumar, P. This work is licensed under a [Creative Commons Attribution-Noncommercial-No Derivatives 4.0 International License](https://creativecommons.org/licenses/by-nc-nd/4.0/).